
Article:
Cholostiakow, S., Di Benedetti, M. orcid.org/0000-0001-7870-1323, Pilakoutas, K. orcid.org/0000-0001-6672-7665 et al. (1 more author) (2019) Effect of beam depth on shear behavior of FRP RC beams. Journal of Composites for Construction, 23 (1). 04018075. ISSN 1090-0268

https://doi.org/10.1061/(ASCE)CC.1943-5614.0000914

Effect of Beam Depth on Shear Behaviour of FRP RC Beams

S. Cholostiakow[1]; M. Di Benedetti[2]; K. Pilakoutas[3]; and M. Guadagnini[4]

[1] Marie Curie Fellow, Dept. of Civil and Structural Engineering, Univ. of Sheffield, Sir Frederick Mappin Bldg., Mappin Street, Sheffield S1 3JD, UK. (corresponding author). Email: s.cholostiakow@sheffield.ac.uk
[2] University Teacher, Multidisciplinary Engineering Education, Univ. of Sheffield, The Diamond, 32 Leavygreave Road, Sheffield S3 7RD, UK.
[3] Professor of Construction Innovation, Dept. of Civil and Structural Engineering, Univ. of Sheffield, Sir Frederick Mappin Bldg., Mappin Street, Sheffield S1 3JD, UK.
[4] Senior Lecturer, Dept. of Civil and Structural Engineering, Univ. of Sheffield, Sir Frederick Mappin Bldg., Mappin Street, Sheffield S1 3JD, UK.

Abstract: The behaviour of shear critical fibre-reinforced-polymer (FRP) reinforced concrete (RC) elements is characterised by the development of comparatively large strains and crack widths, which can be strongly influenced by their relative geometrical size. This paper investigates experimentally the size effect on the shear behaviour of FRP RC beams with and without shear reinforcement and overall depth varying from 260 mm to 460 mm. The results confirm a considerable size effect for members without shear reinforcement, showing an average reduction in normalized shear strength of about 19 %, with maximum value up to 40 %. It is also shown that current design provisions are overall conservative, but with non-uniform margins of safety that decrease with increasing member depth. It is anticipated that the results of this study will help improve the efficiency of future design equations for the shear strength of FRP RC.

Keywords: FRP; reinforced concrete beams; shear strength; size effect; cracking; shear strain; experimental study; diagonal tension failure; shear resisting mechanism.

Introduction

Owing to its non-corrosive characteristics, fibre-reinforced polymer (FRP) reinforcement is primarily used in structures exposed to severe environments, such as bridges. Although FRP reinforcement is widely used in concrete bridge decks (e.g. Morristown Bridge in Vermont, US; Irvine Creek Bridge in Ontario, Canada; Saint Catharine twin overpass bridges in Sherbrook, Canada), FRPs are not used extensively in other bridge elements. This may be attributed to the lack of understanding of shear performance of large FRP reinforced concrete (RC) elements, combined with the overly conservative nature of existing design recommendations, which makes such designs uneconomic (Zoghi 2013).

Even for conventional steel reinforcement, the lack of a universally accepted rational shear theory has led to the development of many simplified empirical design rules, which, although generally conservative, have also been shown to lead to unsafe design, especially for large structural elements, potentially with catastrophic consequences (Burgoyne and Scantlebury 2006; Collins et al. 2008).

The shear performance of large steel reinforced concrete elements has been examined by various researchers (Kani 1967; Shioya et al. 1990; Bazant and Kazemi 1991; Walraven and Lehwalter 1994; Collins and Kuchma 1999; Frosch 2000; Angelakos et al. 2001; Bentz 2005; Hassan et al. 2008, Yu et al. 2013), and it was found that for geometrically similar members shear strength at failure reduces with increasing beam depth; i.e. there is a "size effect". The Joint ASCE and ACI Committee 445 on Shear and Torsion (ASCE-ACI 1998) attributed size effect mainly to a reduction in the resistance offered by aggregate interlock as a result of larger crack openings. Various models based on empirical observations and plasticity theory have been developed over the years to account for size effect (e.g. Reineck 1991; Collins et al. 1996; Lubell et al. 2004) and

implemented in design codes (EN 1992; JSCE 1997; AASHTO 2007; CSA 2004; ISIS 2007; CSA 2012; CSA 2014; Model Code 2010). Other researcher tried to model size effect as a function of energy release at failure caused by macro crack growth (Bazant 1984; Bazant and Kim 1984; Bazant and Kazemi 1991).

Experimental evidence (Nanni 1993; Benmokrane et al. 1995; Alsayed et al. 2000; Yost et al. 2001; Pilakoutas et al. 2002; Razaqpur et al. 2004; Guadagnini et al. 2006; El Sayed et al. 2006) suggests that, although the same resisting mechanisms are mobilised, the shear capacity of FRP RC elements is lower than that of their equivalent steel reinforced concrete counterparts. Under similar loading conditions, FRP RC elements develop much higher deformations, thus exhibiting wider and deeper cracks (Tureyen and Frosh 2002). In turn, larger strain in the FRP flexural reinforcement results in a reduced portion of concrete resisting shear in compression and weakened aggregate interlock along cracks.

Experimental studies on FRP RC elements varied in overall depth (e.g. Matta et al. 2007; Bentz et al. 2010; Alam and Hussein 2012; Ashour and Kara 2014; Mahmoud and El-Salakawy 2016) show that size effect is significant primarily in beams without web reinforcement and is mitigated by the presence of shear reinforcement (Matta et al. 2013). In particular, test results on large beams having effective depth 880 mm and low longitudinal reinforcement ratios (0.09-0.12 %), report a decrease in nominal shear strength up to 65 % (e.g. Matta et al. 2013; Massam 2001) .

Current shear design recommendations for FRP RC (JSCE 1997; BISE 1999; CSA 2012; CNR 2006; ISIS 2007; CSA S6-2014; ACI 2015) are based on modifications of models originally developed for conventional steel RC, but account somehow for the lower stiffness of the FRP bars. Size effect, when included, is modelled through the use of empirically derived parameters calibrated against experimental data collected from steel RC specimens. These assumptions may

potentially result in unsafe design or produce low margins of safety for large FRP RC beams having overall depth greater than 300 mm (Razaqpur and Isgor 2006; Razaqpur et al. 2011).

The aim of the current study is to investigate experimentally the shear behaviour of FRP RC beams with and without shear reinforcement, examining in detail the effect of beam size on crack initiation and development, strain distribution and failure mode. The performance of current design oriented shear models including ACI440.1R-15, CSA S6-2014, CSA 806-12, Hoult et al. (2008) and fib 2007 is also assessed. The results are expected to assist in the development of more reliable shear design equations for large FRP RC members.

Experimental Programme

The experimental programme was designed to investigate size effect on shear behaviour of FRP RC beams with and without shear reinforcement. A total of fifteen tests were carried out on eight FRP RC beams (full details are shown in Fig. 1). The specimens were divided into two groups, comprising beams without shear reinforcement (GB54-GB58, GB58R, GB59R, GB58-0 and GB59-0) and beams with closed external FRP links (GB60-GB65), respectively. The parameters investigated in this study were: effective depth, d; presence of shear links; and concrete strength, f'_c. All other parameters, including beam width, b_w, longitudinal tensile reinforcement ratio, ρ_f, shear-span-to-depth ratio, a/d, were kept constant.

Test Specimens

As summarised in Fig. 1, testing of each beam was carried out in two consecutive phases (except GB58, which was tested only at first phase) so as to allow an in-depth examination of the behaviour of the two shear spans. For instance, tests GB64 and GB65 were performed on the same specimen. During the first phase of testing, the damage was induced primarily on the left shear span, keeping

clear span equal to 2300 mm (see Fig. 1). During the second phase, the shear span tested in the first phase was cut off and the second test was performed on shorter clear span, *a'*=1400 mm, yet keeping the same shear span length, a=900 mm. For beams with the overall depth 460 mm the second phase of testing was performed without cutting off the tested shear span "a" so as to keep the same clear span (2300 mm) during both test phases. In addition, post-tensioned metal straps (PTMS) (Helal et al. 2016) were used to strengthen the tested shear span and, in case of GB61, a cement grout was used to repair the beam before testing. PTMS were also provided along span *a'* of some of the specimens to ensure that failure occurred in the instrumented shear span.

Concrete

The beams were cast in three batches using normal weight ready-mix concrete with a maximum aggregate size of 20 mm, a water-to-cement ratio of 0.55, and cement type 52,5N CEM I. Beams GB58R, GB59R, GB58-0 and GB59-0 were cast using concrete with angular aggregates (limestone), while round river aggregates were used for the remaining beams. The compressive concrete strength was determined on the day of testing from three 100 mm cubes cured under the same conditions as the beams. The concrete cylinder compressive strength, f'_c, was taken as 80 % of the cube compressive strength (Table 1).

FRP Reinforcement

The details and layout of the FRP internal and external reinforcement are shown in Fig. 1 and Table 2-3. The main flexural reinforcement comprised commercially available sand coated GFRP bars (Fig. 2a) with nominal diameter of 12.7 mm (average measured 13.5 mm). The number of bars was selected to prevent flexural failure prior to shear failure, resulting in a longitudinal reinforcement ratio of about 0.85 %. In addition, longitudinal sand coated basalt FRP (BFRP) bars with nominal diameter of 6 mm were used at specific heights within the web of the specimens. It

should be noted that, although the use of skin reinforcement has been shown to mitigate size effect (Collins and Kuchma 1999; Bentz 2010), the BFRP bars used in this study were selected to be sufficiently small to offer negligible contribution to shear resistance, yet enable the installation of strain gauges at various locations of interest within the test spans. Beams GB58-0 and GB59-0 served as control specimens and were constructed without the skin reinforcement to assess the contribution of the BFRP bars to the overall shear capacity of the beams.

External FRP links were employed as shear reinforcement to facilitate the monitoring of deformations and to gain an additional insight into strain distribution along the link length using Digital Image Correlation. The FRP links were wrapped continuously around the beam, with an overlap in the top part of the beam perimeter eliminating the possibility of premature delamination. The external FRP links (Fig. 2b) were manufactured in the laboratory using continuous strips of glass and carbon fibre sheets impregnated with an epoxy resin. The two types of fibres were used to investigate the influence of link stiffness on the cracking and overall shear behaviour of the beams. GFRP links were used in specimens GB60, GB62 and GB64, while CFRP links were used in GB61, GB63 and GB65. The shear reinforcement was designed to provide the minimum shear reinforcement ratio of $\rho_{fv,min}=0.35/f_{fv}$ recommended in ACI 440.1R-15 (Table 3).

Strain developed on the external links can be slightly different than that in equivalent internal links mainly to the expected different bond behaviour. However, given that the links are fully anchored (fully wrapped around the section), once mobilized, their behaviour is expected to be similar to internally placed stirrups. As long as they are effectively anchored, the contribution of shear links can be calculated based on the truss analogy and the effective strength of the links (also a function of the geometry of the bent portions). The shear depth considered in design (i.e. the distance between the centroid of the area of concrete in compression and the tension reinforcement) is only

determined by the position of the flexural reinforcement. This is also reflected in current design approaches for internal and external links.

Test Setup and Instrumentation

All beams were simply supported and tested in an asymmetric 3-point bending configuration. The load was applied in displacement control at a rate of 0.25 mm/min. The dimensions of loading and bearing steel plates were identical and equal to 75x150x20 mm. The loading procedure consisted of two load cycles followed by a final load ramp up to failure. The cycles were performed at load levels inducing strain in the main longitudinal reinforcement of about 3,000 με and 4,500 με, which were taken as the strain levels expected under typical service conditions and corresponding to the maximum allowable strain limit in the reinforcement, respectively. Specimens with overall depth of 460 mm failed during the second cycle before the target strain of 4,500 με could be attained.

The typical test setup is shown in Fig. 3a (GB65). The instrumentation was designed to measure load, vertical displacement of the beam and strains in the FRP reinforcement. The deflection profile of the beam was measured by 3 potentiometers placed under the loading point and at the middle of each shear span. To account for any support movement, two additional potentiometers were used to measure the displacement at each support. Strain in the reinforcement was monitored by electrical resistance strain gauges (5 and 10 mm length for the BFRP and GFRP bars, respectively) bonded to the longitudinal reinforcement on a grid of 150 mm and distributed spatially so as to capture the initiation and development of the expected shear crack (Fig. 3b). Additional gauges were installed on the FRP shear links to enable a more accurate estimate of their contribution to shear resistance.

Test Results and Discussion

The main results obtained in the experimental program are summarized in Table 4. All beams exhibited a brittle diagonal tension shear failure caused by the development of diagonal cracks (Fig. 4).The shear cracks initiated from flexural cracks within the shear span (see white circles in Fig. 4) and propagated towards the compression zone under the loading point. The location of the initiation point depended on the member size and, the taller the beam, the lower the initiation point. For instance, the onset of the shear crack in GB58 and GB62 was almost at mid-height of the beam (0.61d and 0.55d, respectively), whereas in GB56 and GB60 it was near the level of the tensile reinforcement (0.87d and 0.78d, respectively). As the load increased, the flexural cracks propagated higher and additional smaller cracks developed from and along the shear crack. Just before failure, the shear crack "pushed" the bottom concrete cover off and propagated along the longitudinal reinforcement towards the support.

The diagonal shear failure of the members reinforced with shear links was abrupt and caused the rupture of the links. The fracture usually started from the link closest to the initiation point. No premature failure of the links due to debonding or anchorage failure was observed in any of the beams.

Load-Deflection Behaviour and Stiffness

The plots of shear load (in the critical span) versus net deflection under the loading point for all beams are shown in Fig. 5. Each plot compares the response of beams tested under the same setup. The black and red curves represent the beams without shear links, while the grey curves correspond to the beams with shear links. The beams without skin reinforcement GB58-0 and GB59-0 (red curves) developed shear in the tested span about 5 kN lower than the corresponding beams with the mid-height bars. This indicates that basalt bars at the mid-height of the beam slightly

contributed to shear and helped maintain beam stiffness after development of the critical shear crack. However, this additional strength is expected to decrease in larger members due to larger and deeper shear cracks and is not expected to affect significantly the overall shear capacity. In general, the shear capacity of the beams without shear links increased with increasing member depth. Only GB54 developed slightly lower (about 15 %) shear capacity than its scaled counterparts GB58 and GB58R. Although within the expected variability of results, this can be mainly attributed to the lower strength measured for the concrete of GB54 (30.1 MPa).

The higher concrete strength of beams GB62-GB65 affected both stiffness and cracking behaviour. In general, an increase in the stiffness and cracking load was observed when compared to beams without shear links. The higher stiffness and capacity exhibited by GB65 in comparison to GB55 can be attributed to the ability of the shear links to control diagonal crack opening along the test span, thus enabling the further development of a stiffer truss-like transfer mechanism. On the other hand, GB60 and GB61 showed very similar initial shear load-deflection behaviour to the beams without shear links (GB56 and GB57), but developed a higher shear capacity through the contribution of the shear reinforcement.

The critical shear span length was kept identical in both testing phases and, as expected, a similar shear resistance was recorded, with differences usually not exceeding 10 %. However, GB55 developed a shear strength almost 35 % higher than GB54. This suggests that the relative length of the shear spans might have an influence on the overall behaviour and relative contribution of the resisting mechanisms. Such behaviour could be a result of material's natural variability but warrants further investigations.

Crack Development

Fig. 6 shows the crack patterns for all beams along with the values of the angles of the main shear cracks estimated at mid-height. In general, analogous crack patterns were observed for geometrically equivalent elements. However, the beams with GFRP links (first phase tests) showed steeper shear crack inclinations in comparison to the unreinforced beams. This confirms that the shear links were effectively engaged and able to control the opening of the shear cracks. Crack spacing increased with member depth, which is in agreement with the observations from other studies (e.g. Alam and Hussein 2012).

Strains in Reinforcement

The strain recorded in the main reinforcement under the loading point for the first and second phase of testing is shown in Fig. 7a and Fig. 7b, respectively. The maximum allowable strain of 4500 με proposed in Guadagnini et al. (2003) is indicated in the Figure with dashed lines. All beams with overall depth 360 mm (green curves) and 260 mm (red curves) exceeded this strain, which confirms that this strain limit provides a reasonable margin of safety for beams of this size and smaller. However, strain levels of 4,100 με and 4,500 με were recorded for GB56 and GB57, thus indicating that the strain limit of 4,500 με may not be suitable for larger FRP RC beams without shear reinforcement and, hence, needs to be reassessed.

Fig. 8, Fig. 9 and Fig. 10 show the strain distributions at different shear load levels (indicated with different markers) for beams GB58, GB54 and GB56. The top graphs plot strain in the longitudinal bars (B, C and D) along the beam length, while the bottom ones show the strain profiles over beam depth at various sections. The red dashed lines correspond to strain at failure load estimated using cross-section analysis. The highest strain values were recorded in the lateral BFRP bars near the location of the main shear crack, usually at about mid-height of the beam (bar B in GB58 and

GB54 and bar C in GB56). As can be observed, strains measured in different reinforcement layers did not change linearly within the beam height as it is expected from the plane section principle, both at sections crossing a shear crack (sections 3-3 and 4-4) and at those where maximum bending moment was attained (1-1). The strain in the main GFRP reinforcement immediately below the load (section 1-1) was close to that estimated by cross-section analysis (red dashed lines), while strain values in the lateral BFRP bars at mid-height were largely underestimated (see strain profiles in Fig. 8, Fig. 9 and Fig. 10). The high strain values recorded at mid-depth of the tested beams were significantly higher than those predicted by beam theory only within the disturbed regions of the beams, which were subjected to a high interaction of shear and bending. However, these measurements are local and do not necessarily conflict with the assumption that plane sections can be considered to remain plane in undisturbed regions. Disturbance of plane section strains due to shear cracks is well known and additional deformations due to shear cracks have been documented (e.g. Imjai et al. 2016). The local strain measurements are also affected by the bond between the bars used in the test and the surrounding concrete. In contrast, strain profiles of relatively undamaged sections not subjected to large shear deformations (1'-1' and 3'-3'), were similar to the analytical predictions, showing a linear trend along the beam depth.

Fig. 11 shows the strain distribution of GB62 as representative of the typical behaviour observed for all of the tested beams with external GFRP shear links. The strain distribution is similar to that of its unreinforced counterpart (GB58), albeit higher strains were obtained after shear cracks developed. For shear loads above 30 kN, when the shear crack started to form, GB62 developed slightly higher strain values than GB58 at mid-height of section 1-1 (of about 1,000 με), while much larger strains were recorded at ultimate (up to 13,000 με). A similar shift in strain values after shear cracking (about 1,500 με) was observed in GB64 and GB54, thus providing evidence

that shear links effectively controlled the opening of the diagonal cracks and changed the strain distribution along the beam span and across the beam height. In fact, shear links successfully reduced strains in the section across the shear crack. For instance, GB62 recorded no strains at mid-height of the critical section 3-3 up to a load of 35 kN. In contrast, the strain values measured in GB58 at the same load level were above 9,000 με and the beam was approaching failure.

Fig. 12 shows the strain distribution in the GFRP links of beam GB60, which is representative of what was experimentally observed in all other specimens. The beam failed by rupture of link 3 in the region where the shear crack was the widest and strain values reached about 16,800 με. The full-field map of vertical strain obtained from DIC (bottom image in Fig. 12) clearly shows that no significant strains were recorded in the links along the un-cracked areas, thus indicating good bond between the concrete and the FRP links and effective anchorage of the shear reinforcement.

Effect of Member Depth

Fig. 13 shows the normalized shear strength as a function of beam effective depth. As can be seen, size effect is observed in the beams without shear links, and a reduction up to 40 % can be observed between minimum and maximum experimental values (Fig. 13a). However, the average size effect in beams having mid-height BFRP bars (grey markers) is about 19 %. This seems to be in agreement with results published by Alam and Hussein (2012) who reported a strength decrease of 20 % for similarly reinforced specimens with effective depths ranging from 305 mm to 440 mm. The scattered values of shear strength in Fig. 13a (in particular for the shallowest members) may be mainly attributed to material variability and the geometry of the critical shear crack. It is worth noting that the tests performed on the two beams without mid-height BFRP reinforcement (red markers) showed an average reduction in shear strength of about 10 % and an increase in the angle of the shear crack (see Fig. 6a) with respect to the same beams with mid-height bars. This shows

that such bars can help resisting shear; however, not necessarily eliminating size effect. On the other hand, the presence of shear links mitigates effectively size effect (Fig. 13b) and reduces the variability in the results.

Although the beams investigated in this study do not cover large-scale elements, the observed decrease in normalized shear strength is aligned with that observed in studies examining a wider range of beam depths. For instance, Bentz et al. (2010) reported size effect up to 32 % in beams with an average reinforcement ratio of 0.44 % as the effective depth is increased from 188 mm to 860 mm. Matta et al. (2013) observed a strength decrease up to 36 % between beams having effective depths varying from 146 mm to 880 mm and flexural reinforcement ratio of 0.24 %.

Discussion and Comparison of Results

Existing shear design approaches for FRP RC estimate the total shear capacity of an element by considering the contribution of both concrete (V_c) and shear links (V_f). However, this is true only when shear crack openings (notably larger in FRP RC than in steel RC) are controlled, and all shear resisting mechanisms are effectively mobilised. This is included implicitly in current guidelines by imposing strain limits on shear reinforcement. However, as discussed in the following, current design guidelines (e.g. ACI Committee 440 2015, CSA S6 2014, CSA S806 2012, fib bulletin 40 2007) recommend different limiting strain values and adopt different models to estimate the contribution of concrete (V_c).

In ACI, the total shear contribution is given by the sum of the following equations:

$$V_c = \frac{2}{5}\sqrt{f'_c}\, b_w d k \tag{1}$$

$$V_f = \frac{A_{fv}\, f_{fv}\, d}{s}; \qquad f_{fv} = 0.004 E_f \le f_{fb} \tag{2}$$

In this approach, the allowable stress in the shear reinforcement is the minimum between the stress corresponding to a strain level of 0.4 % and the maximum stress level that can be developed at the

bent portion of the link (f_{fb}). In addition, the inclination of the concrete strut is assumed to be 45 degrees and no provision for size effect is included.

The CSA design equation recognizes size effect only in concrete members without transverse reinforcement having effective depth greater than 300 mm (k_s). In addition, the code equations account for the flexure-shear interaction (k_m) and limit the maximum strain in the shear links to 0.5 %. The angle of the concrete strut is calculated using Eq. 5. The contribution of both concrete and shear reinforcement is calculated as a sum of the following:

$$V_c = 0.05\lambda\phi_c k_m k_r k_s f'^{1/3}_c b_w d_v \quad (3)$$

$$V_f = \frac{0.4\phi_F A_{fv} f_{fu} d_v}{s}\cot\theta \quad (4)$$

where the inclination of the concrete strut θ is calculated as following:

$$30° \le \theta = 30 + 7000\varepsilon_x \le 60° \quad (5)$$

The Canadian Highway Bridge Design Code (CHBDC) CSA S6 2014 recommends calculating the total shear resistance of FRP RC beams reinforced with external fully wrapped links as a sum of the following:

$$V_c = \beta\phi_C \sqrt{f'_c} b d_v \quad (6)$$

$$V_f = \frac{\phi_{FRP} E_{FRP} 0.004 A_{FRP} d_{FRP} \cot\theta}{s_{FRP}} \quad (7)$$

This model relies on the modified compression field theory (MCFT) and it is based on a variable angle truss model and a variable concrete contribution. The parameter β models the ability of concrete to transmit tensile stresses, and for FRP reinforced concrete sections should be computed using the general method (Eq. 8).

$$\beta = \left(\frac{0.4}{1+1500\varepsilon_x}\right)\left(\frac{1300}{1000+s_{ze}}\right) \quad (8)$$

The longitudinal strain at mid-depth, ε_x, for the specimens presented in this study was calculated as follows:

$$\varepsilon_x = \frac{\frac{M_a}{d_v} + V_a}{2(A_{fl} E_{fl})} \leq 3{,}000\,\mu\varepsilon \tag{9}$$

where M_a and V_a correspond to the applied moment and the shear force at failure at a distance d_v from the loading. The contribution of shear links is calculated assuming that FRP shear links are fully anchored in the compression zone and maximum strain in the links is limited to 0.4 %. The inclination of the shear crack was calculated as follows:

$$\theta = (29 + 7000\varepsilon_x)(0.88 + s_{ze}/2500) \tag{10}$$

The accuracy of Eq. 6 can be further improved using a refined "second order" MCFT algorithm (Hoult et al. 2008)(Eq. 11), which was derived to account for the larger strains typically attained in FRP RC beams at ultimate.

$$V_c = \left(\frac{0.3}{0.5 + (1000\varepsilon_x + 0.15)^{0.7}}\right)\left(\frac{1300}{1000 + s_{ze}}\right)\sqrt{f'_c}\,b d_v \tag{11}$$

The theoretical shear resistance of the tested beams is also calculated using the "Sheffield Approach" (Guadagnini et al. 2003) as included in fib bulletin 40 (fib 2007), and accounting for the different stiffness of the FRP tensile reinforcement through the modular ratio E_f/E_s. A ratio of 1.8 is also introduced to account for the higher strain that can be developed in the FRP longitudinal reinforcement upon shear failure (4,500 με) when compared to the level of strain that can be mobilized at yielding in the more conventional steel reinforcement (about 2,500 με). The same strain limit of 4,500 με (0.45%) was also adopted to calculate the contribution of the links and a fixed crack inclination of 45° was assumed (Eq. 13). The design equations are shown below:

$$V_c = \left[\frac{0.18}{\gamma_c} \cdot \left(1 + \sqrt{\frac{200}{d}} \right) \cdot (100 \frac{A_{fl}}{b_w d} \cdot \frac{E_{fl}}{E_s} \cdot 1.8 \cdot f_{ck})^{\frac{1}{3}} \right] b_w d \quad (12)$$

$$V_f = \frac{A_{fv}}{s} 0.0045 E_{fv} z \quad (13)$$

The theoretical predictions for all tested beams are shown in Table 5. For the sake of comparison, all safety and material factors were omitted in the calculations. As can be seen, the models examined tend to produce conservative results and significantly underestimate the shear capacity of the tested elements. The ACI equation yields the most conservative predictions with an average experimental-to-theoretical shear capacity ratio for beams without reinforcement above 2.0, while the best correlation was obtained when fib 2007 and CSA 2012 model was used. The mean value of V_{exp}/V_{calc} obtained using the CHBDC method was equal to 1.83 for the beams without shear links, which is in agreement with the findings of other researchers (El-Sayed and Benmokrane 2008; Mahmoud and El-Salakawy 2015). The implementation of Hoult et al. (2008) model yielded a better estimate of the shear capacity of beams without shear links with an average V_{exp}/V_{calc} ratio of 1.21.

The normalized shear strength predicted by ACI for the beams without shear reinforcement (square markers in Fig. 13a) is almost constant as no size effect parameter is included in the original formulation, and the only deviations are caused by the slightly different reinforcement ratios. Although size effect is accounted for in the CHBDC equation (Eq. 8), the observed values of normalized shear strength are similar to those derived using the ACI equation. The conservative predictions can be mainly attributed to the fact that the higher values of strain calculated in the FRP flexural reinforcement result in low values of β. The model proposed by Hoult et al. (2008) attempts to address this issue and yields less conservative results (diamond markers in Fig. 13a). The use of CSA and fib (cross and triangular markers, respectively, in Fig. 13a) yielded similar

predictions for the beams without shear reinforcement and produced estimates close to the average of the experimental values. However, both are still conservative in their predictions of the beams with shear reinforcement, with the fib producing the best results (Fig. 13b). The high degree of safety can be partly attributed to the conservative values adopted as limiting strain for shear reinforcement as well as conservative assumptions for calculating V_f using CSA 2012. The experimental strain values recorded at failure in the links ranged from about 9,000 με to 16,800 με for GFRP links and from about 6,800 με to 13,500 με for CFRP links (see Tab. 4), and are much higher than the limitations specified in current design recommendations (ranging from 4,000 με to 5,000 με). This provides further evidence that the contribution of shear links to overall shear resistance can be substantially underestimated by the current FRP design codes. It should be noted that the local strain measured on the externally bonded links adopted in this research programme is expected to be lower than the maximum strain that would be developed in internal links (due to local debonding) and, hence, can still be used to inform the selection of design limiting values. When considering the adoption of less conservative limiting values, however, it should be kept in mind that high strain values in FRP links result in larger crack widths and degradation of the shear resisting mechanisms, thus leading to an overall reduction in shear capacity.

The relative shear strength of shear-reinforced beams did not change when increasing beam depth (though it shows variability). This may be attributed to the ability of the shear links to effectively control cracking and maintain an adequate level of shear transfer across the cracks. For instance, at an applied shear force of approximately 30 kN, a maximum crack width of 1.8 mm was observed in the shear span of GB58, whilst the maximum crack width for GB62 and GB63 at the same load level was only 0.3 mm and 0.2 mm, respectively. In beams with larger depth, the difference in shear crack width at comparable levels of applied shear force between beams without and with

shear reinforcement was less pronounced, e.g. 0.6 mm for GB56 and 0.4 mm for GB60. This suggests that the relative contribution of concrete and shear reinforcement to the overall shear capacity is also a function of beam depth.

Conclusions

Fifteen shear tests were performed on FRP RC beams with and without shear reinforcement to investigate their shear behaviour with a specific focus on the effect of beam depth. The experimentally determined distribution of both horizontal and vertical strain within the shear span of the tested beams was presented and discussed. The results were compared with the predictions obtained from current design equations to verify their accuracy in terms of overall capacity and contributions of different resisting mechanisms. From the discussion and results presented in this study, the following conclusions can be drawn:

- All tested beams failed in diagonal tension. The depth at which flexural cracks transition to diagonal shear cracks is a function of the overall depth of the beams. In particular, the taller the beam, the lower the depth of initiation of the diagonal crack. As already observed in steel RC beams, crack spacing was confirmed to be a function of beam size, with larger spacing being developed in deeper specimens.
- The maximum strain in the FRP reinforcement (both flexural and shear) generally exceeded allowable design limits. A decrease in the maximum strain developed in the flexural reinforcement was observed with increasing member depth. The maximum values measured in the flexural reinforcement ranged from 4,100 με to 7,900 με in beams without shear links and from 8,300 με to 12,000 με in beams with shear links. The maximum strain in the shear reinforcement ranged from 9,000 με to 16,800 με for GFRP links and from 6,800 με to 13,500 με for CFRP links.

- Although the same a/d ratio was maintained for the test shear-span of all specimens, the relative stiffness of the shear spans appears to affect overall performance and relative shear strength. Such behaviour has not been reported in previous literature and could be a result of material's natural variability but requires further investigation.
- Current FRP design equations do not predict the shear strength of FRP RC beams of different sizes with a uniform margin of safety.
- The results confirm that shear strength of FRP members without shear links is somehow affected by their size. The CSA (2012) and fib (2007) models account for this sufficiently, while ACI and CHBDC (CSA 2014) predictions are overly conservative. The model proposed by Hoult et al. (2008) yields a better estimate of V_c than the equation originally implemented in CHBDC. No significant size effect is found in beams with shear reinforcement, which appears to control crack width sufficiently, even at larger strains than allowed by current design models. Overall, the model included in fib 2007 predicts reasonably well the performance of shear-reinforced beams, even though the relative contribution of individual shear resisting mechanisms needs to be re-examined.

Acknowledgments

This research was funded by the EU FP7 Marie Skłodowska - Curie Initial Training Network endure (grant agreement n.607851). The authors would like to thank the European Commission for its financial support and for providing wide networking opportunities within the research community.

Notation

The following symbols are used in this paper:

A_{fl} = total area of the longitudinal reinforcement;

A_{fv} = total area of the shear reinforcement at given spacing;

a = length of the test shear span;

a' = length of the non-test shear span;

b_w = width of the beam;

d = effective depth of the beam;

d_v = effective shear depth of the beam;

E_c = modulus of elasticity of the concrete;

E_{fl} = Young's modulus of longitudinal FRP reinforcement;

f'_c = concrete cylinder strength;

f_{fv} = allowable stress in the shear reinforcement;

h = overall depth of the beam;

k_1 = ratio between the shear load in the test shear span and applied load;

M_a = applied moment;

P_{ult} = ultimate load applied;

s = spacing of the FRP shear links;

s_{ze} = effective crack spacing;

V_a = applied shear force;

V_c = calculated shear strength provided by concrete;

V_{exp} = experimental shear capacity;

V_f = calculated shear strength provided by shear links;

β = factor depending on ability of concrete to transmit tensile stresses;

ε_x = strain at beam mid-depth;

$\varepsilon_{l,max}$ = maximum strain in the main longitudinal reinforcement;

$\varepsilon_{t,max}$ = maximum strain in the shear links;

θ = angle of inclination of the principal diagonal compressive stresses;

ρ_{fl} = longitudinal reinforcement ratio;

References

AASHTO. (2007). LRFD Bridge design specifications, 4th Ed., Washington, DC.

ACI (American Concrete Institute). (2015). "Guide for the design and construction of structural concrete reinforced with FRP bars." ACI 440.1R-15, Farmington Hills, MI.

Alam, M. S., and Hussein, A. (2012). "Size effect on shear strength of FRP reinforced concrete beams without stirrups." J. Compos. Constr., 10.1061/(ASCE)CC.1943-5614.0000346, 507-516.

Alsayed, S. H., Al-Salloum, Y. A., and Almusallam, T. H. (2000). "Performance of glass fiber reinforced plastic bars as a reinforcing material for concrete structures." Compos. Part B., 31(6), 555-567.

Angelakos, D., Bentz, E. C., and Collins, M. P. (2001). "Effect of concrete strength and minimum stirrups on shear strength of large members." J. Struct. Eng., 98(3), 290–300.

Ashour, A. F., and Kara, I. F. (2014). "Size effect on shear strength of FRP reinforced concrete beams." Compos. Part B., 60, 612-620.

Bazant, Z. P. (1984). "Size effect in blunt fracture: concrete, rock, metal." J. Eng. Mech., 110(4), 518-535.

Bazant, Z. P., and Kazemi, M. T. (1991). "Size effect on diagonal shear failure of beams without stirrups." ACI Struct. J., 88(3), 268-276.

Bazant, Z. P., and Kim, J. K. (1984). "Size effect in shear failure of longitudinally reinforced beams." ACI Journal., 8, 456-468.

Benmokrane, B., Chaallal, O., and Masmoudi, R. (1995). "Glass fibre reinforced plastic (GFRP) rebars for concrete structures." Constr Build. Mater., 9(6), 353-364.

Bentz, E. C. (2005). "Empirical modeling of reinforced concrete shear strength size effect for members without stirrups." ACI Struct. J., 102(2), 232.

Bentz, E. C., Massam, L., and Collins, M. P. (2010). "Shear strength of large concrete members with FRP reinforcement." J. Compos. Constr., 10.1061/(ASCE)CC.1943-5614.0000108, 637-646.

BISE (British Institution of Structural Engineers). (1999) "Interim guidance on the design of reinforced concrete structures using fiber composite reinforcement". IStructE, SETO Ltd., London, UK.

Burgoyne, C. J., and Scantlebury, R. (2006). "Why did Palau Bridge collapse?" The Structural Engineer, 84. pp. 30-37. ISSN 0039-2553

Collins, M. P., and Kuchma, D. (1999). "How safe are our large, lightly reinforced concrete beams, slabs, and footings? " ACI Struct. J., 96(4), 482-490.

Collins, M. P., D. Mitchell, and E. C. Bentz. (2008). "Shear design of concrete structures." The Structural Engineer., 86.10, 32-39.

Collins, M. P., Mitchell, D., Adebar, P., and Vecchio, F. J. (1996). "A general shear design method." ACI Struct. J., 93(1), 36-45.

Comité Européen de Normalisation (CEN). (2004). "Eurocode 2: Design of Concrete Structures: Part 1-1: General Rules and Rules for Buildings" EN 1992-1-1, Brussels, Belgium.

CSA (Canadian Standards Association). (2012). "Design and construction of building structures with fibre-reinforced polymers." S806-12, Mississauga, ON, Canada.

CSA (Canadian Standards Association). (2014). "Canadian Highway Bridge Design Code." CSA S6-14, Mississauga, ON, Canada.

El-Sayed, A. K., and Benmokrane, B. (2008) "Evaluation of the new Canadian highway bridge design code shear provisions for concrete beams with fiber-reinforced polymer reinforcement." Can. J. Civ. Eng. 35, 6, 609-623.

El-Sayed, A. K., El-Salakawy, E. F., and Benmokrane, B. (2006). "Shear strength of FRP-reinforced concrete beams without transverse reinforcement." ACI Struct. J., 103(2), 235.

fib (Fédération internationale du béton). (2007). "FRP reinforcement in RC structures, technical". fib bulletin 40, Technical report. Lausanne, Switzerland.

fib (Fédération internationale du béton). (2013). "Model Code for Concrete Structures 2010". Ernest&Sohn, ed., Weinheim.

Frosch R. J. (2000). Behavior of large-scale reinforced concrete beams with minimum shear reinforcement ACI Struct. J., 97(6), 814-820.

Guadagnini, M., Pilakoutas, K., and Waldron, P. (2003). "Shear performance of FRP reinforced concrete beams." J. Reinf. Plast. Compos., 22(15), 1389-1407.

Guadagnini, M., Pilakoutas, K., and Waldron, P. (2006). "Shear resistance of FRP RC beams: Experimental study." J. Compos. Constr., 10.1061/(ASCE)1090-0268(2006)10:6(464), 464-473.

Hassan, T. K., Seliem, H. M., Dwairi, H., Rizkalla, S. H., and Zia, P. (2008). "Shear behavior of large concrete beams reinforced with high-strength steel." ACI Struct. J., 105(2), 173.

Helal, Y., Garcia, R., Pilakoutas, K., Guadagnini, M., and Hajirasouliha, I. (2016). "Strengthening of short splices in RC beams using Post-Tensioned Metal Straps." Mater. Struct., 49(1-2), 133-147.

Hoult, N. A., Sherwood, E. G., Bentz, E. C., and Collins, M. P. (2008). "Does the use of FRP reinforcement change the one-way shear behavior of reinforced concrete slabs?" J. Compos. Constr., 10.1061/(ASCE)1090-0268(2008)12:2(125), 125-133.

Imjai, T., Guadagnini, M., Garcia R. and Pilakoutas, K. (2016) "A practical method for determining shear crack induced deformation in FRP RC beams." Eng. Struct. 126, 353-364.

ISIS Canada. (2007). "Reinforcing concrete structures with fiber reinforced polymers." ISIS-M03-07, Canadian Network of Centers of Excellence on Intelligent Sensing for Innovative Structures, Univ. of Winnipeg, Winnipeg, Canada.

Joint ACI-ASCE Committee 445, "Recent Approaches to Shear Design of Structural Concrete." J. Struct. Eng.-ASCE, V. 124, No. 12, Dec. 1998, 1375-1417.

JSCE (Japan Society of Civil Engineers). (1997). "Recommendation for design and construction of concrete structures using continuous fiber reinforcing materials." Concrete Engineering Series 23, A. Machida, ed., Tokyo, Japan.

Kani, G. (1967). "How safe are our large reinforced concrete beams? " In Journal Proceedings., 64, 3, 128-141).

Lubell, A., Sherwood, T., Bentz, E., and Collins, M. (2004). "Safe shear design of large wide beams." Concrete International., 26(1), 66-78.

Mahmoud, K., and El-Salakawy, E. (2015) "Shear strength of glass fiber reinforced polymer–reinforced concrete continuous beams without transverse reinforcement." Can. J. Civ. Eng. 42, 12, 1073-1082.

Mahmoud, K., and El-Salakawy, E. (2016). "Size Effect on Shear Strength of Glass Fiber-Reinforced Polymer-Reinforced Concrete Continuous Beams." ACI Struct. J., 113(1), 125.

Matta, F., El-Sayed, A. K., Nanni, A., and Benmokrane, B. (2013). "Size effect on concrete shear strength in beams reinforced with fiber-reinforced polymer bars." ACI Struct. J., 110(4), 617.

Matta, F., Nanni, A., Galati, N., and Mosele, F. (2007). "Size effect on shear strength of concrete beams reinforced with FRP bars." Proc., 6th International Conf. on Fracture Mech. of Concr. and Concr. Struct. (FraMCoS-6)., Balkema/Taylor & Francis, ed., Vol. 2, pp. 17-22.

Massam, L., "The Behaviour of GFRP Reinforced Concrete Beams in Shear." MSc thesis, University of Toronto, Toronto, ON, Canada, 2001, 304 pp.

Nanni, A. (1993). "Flexural behavior and design of RC members using FRP reinforcement." J. Struct. Eng., 119(11), 3344-3359.

National Research Council. (2006). "Guide for the design and construction of concrete structures reinforced with fiber-reinforced polymer bars." CNR-DT 203, Rome, Italy.

Pilakoutas, K., Neocleous, K., and Guadagnini, M. (2002). "Design philosophy issues of fiber reinfored polymer reinforced concrete structures." J. Compos. Constr., 10.1061/(ASCE)1090-0268(2002)6:3(154), 154-161.

Razaqpur, A. G., Isgor, B. O., Greenaway, S., and Selley, A. (2004). "Concrete contribution to the shear resistance of fiber reinforced polymer reinforced concrete members." J. Compos. Constr., 10.1061/(ASCE)1090-0268(2004)8:5(452), 452-460.

Razaqpur, A. G., and Isgor, O. B. (2006). "Proposed shear deign method for FRP-reinforced concrete members without stirrups." ACI Struct. J., 103(1), 93–102.

Razaqpur, A. G., Shedid, M., and Isgor, B. (2010). "Shear strength of fiber-reinforced polymer reinforced concrete beams subject to unsymmetric loading." J. Compos. Constr., 10.1061/(ASCE)CC.1943-5614.0000184, 500-512.

Reineck, K.-H. (1991). "Ultimate shear force of structural concrete members without transverse reinforcement derived from a mechanical model." ACI Struct. J. 88, (5), 592-602.

Serbescu, A., Guadagnini, M., and Pilakoutas, K. (2014). "Mechanical characterization of basalt FRP rebars and long-term strength predictive model." J. Compos. Constr., 10.1061/(ASCE)CC.1943-5614.0000497, 04014037.

Shioya, T., Iguro, M., Nojiri, Y., Akiyama, H., and Okada, T. (1990). "Shear strength of large reinforced concrete beams." Special Publication, 118, 259-280.

Tureyen, A. K., and Frosch, R. J. (2002). "Shear tests of FRP-reinforced concrete beams without stirrups."Struct. J., 99(4), 427-434.

Walraven, J., and Lehwalter, N. (1994). "Size effect in short beams loaded in shear." ACI Struct. J., 91(5), 585–593.

Yost, J. R., Gross, S. P., and Dinehart, D. W. (2001). "Shear strength of normal strength concrete beams reinforced with deformed GFRP bars." J. Compos. Constr., 5(4), 268-275.

Yu, L., Che, Y., and Song, Y. (2013). "Shear Behavior of Large Reinforced Concrete Beams without Web Reinforcement." Adv Struct Eng., 16(4), 653-665.

Zoghi, M. (2013). The international handbook of FRP composites in civil engineering, CRC Press, Boca Raton, Florida.

List of Figures

Fig. 5. Shear load-deflection plots for all beams. Values in parentheses correspond to compression strength of concrete f'_c (in MPa).

Fig. 6. Crack patterns for all beams: (a) beams without shear reinforcement; (b) beams with shear links.

Fig. 7. Shear load-strain behaviour for all beams: (a) first phase of testing; (b) second phase of testing.

Fig. 8. Strain distribution in beam GB58 (at a given shear load in test shear span).

Fig. 9. Strain distribution in beam GB54 (at a given shear load in test shear span).

Fig. 10. Strain distribution in beam GB56 (at a given shear load in test shear span).

Fig. 11. Strain distribution in beam GB62 (at a given shear load in test shear span).

Fig. 12. Strain distribution along the GFRP shear links of beam GB60 just before failure (at applied load P_{exp}=147kN).

Fig. 13. Size effect on normalized shear strength (a) beams without shear reinforcement; (b) beams with shear reinforcement.

Table 1. Specimen geometry and concrete properties

Specimen	a (mm)	*a'* (mm)	h (mm)	d (mm)	a/d (mm)	*a'/d* (mm)	f'_c (MPa)	E_c [a] (GPa)	ρ_f (%)	Type of links	s (mm)
GB58-0	620	1680	260	233	2.65	7.2	41.6	30.3	0.82	-	-
GB59-0		1060				4.6	48.4	32.7		-	-
GB58		1680				7.2	36.6	28.4		-	-
GB58R		1680				7.2	47.0	32.2		-	-
GB59R		1060				4.6	48.6	32.7		-	-
GB62		1680				7.2	52.7	34.4		GFRP	120
GB63		1060				4.5	50.9	32.4		CFRP	
GB54	900	1400	360	333	2.70	4.2	30.2	28.5	0.86	-	-
GB55		500				1.5	30.2	28.5		-	-
GB64		1400				4.2	47.5	32.4		GFRP	160
GB65		500				1.5	47.5	32.4		CFRP	
GB56	1120	1180	460	433	2.58	2.7	38.0	29.0	0.88	-	-
GB57							36.6	28.4		-	-
GB60							38.4	29.1		GFRP	260
GB61							38.4	29.1		CFRP	

[a] Calculated according to ACI 440.1R-15.

Table 2. Mechanical properties of the FRP longitudinal reinforcement

Flexural bars	Bar diameter (mm)	Cross-sectional area (mm^2)	Modulus of elasticity (GPa)	Tensile strength (MPa)
GFRP bars	13.5	143.0	46.0	758
BFRP bars[a]	6.0	28.3	42.0	1,297

[a] Data from Serbescu et al. 2014

Table 3. Mechanical properties of the FRP shear reinforcement

Shear links in specimens	Type	f_{fv} [a] (MPa)	Cross-sectional area[a] (mm^2)	Modulus of elasticity[a] (GPa)	Tensile strength[a] (MPa)
GB60	GFRP	260	40.5	65	1,700
GB61	CFRP	964	10.5	241	4,140
GB64	GFRP	260	28.4	65	1,700
GB65	CFRP	964	8.4	241	4,140
GB62	GFRP	260	21.6	65	1,700
GB63	CFRP	964	6.3	241	4,140

[a] Determined for dry fibres

Table 4. Main test results

Beam	$\varepsilon_{l,max}$ (με)	$\varepsilon_{t,max}$ (με)	P_{ult} (kN)	k_1	V_{exp} (kN)	v_{norm} (MPa)	θ_{exp} (deg)	Eq.5 (deg)	Eq.10 (deg)
GB58-0	7,100	-	38.9	0.73	28.4	0.13	60	52	48
GB59-0	6,600	-	39.8	0.63	25.1	0.10	56	50	47
GB58	7,100[a]	-	51.0	0.73	37.3	0.18	40	59	48
GB58R	7,900[a]	-	47.2	0.73	34.4	0.14	45	57	48
GB59R	6,700[a]	-	47.8	0.63	30.2	0.12	50	54	48
GB62	11,000[a]	12,900	66.1	0.73	48.2	0.19	60	60	48
GB63	12,000[a]	6,800	86.0	0.63	54.2	0.22	45	60	48
GB54	4,400[a]	-	51.5	0.61	31.3	0.11	52	47	46
GB55	5,500[a]	-	132.5	0.36	47.3	0.17	50	55	50
GB64	10,000	9,000	101.4	0.61	61.7	0.18	59	60	50
GB65	8,900[b]	10,500	177.5	0.36	63.4	0.18	50	60	50
GB56	4,100[a]	-	85.6	0.51	43.9	0.11	44	47	47
GB57	4,500[a]	-	97.4		50.0	0.13	40	49	50
GB60	8,300[a]	16,800	150.5		77.2	0.19	53	60	52
GB61	x	13,500	166.4		85.4	0.21	45	60	52

Note: x = gauge did not work
[a]Average value from two strain gauges placed on opposite side of the beam
[b]Value presents the last reading from the gauge at shear load of about 60 kN

Table 5. Code predictions

Beam	ACI 440.1R-15		fib 2007		CSA S 806-12		CSA S6 2014		Hoult et al. 2008	ACI 440.1R-15		fib 2007		CSA S 806-12		CSA S6 2014		Hoult et al. 2008
	V_c	V_f	V_c	V_f	V_c	V_f	V_c	V_f	V_c	V_{exp}/V_c	V_{exp}/V_c+V_f	V_{exp}/V_c	V_{exp}/V_c+V_f	V_{exp}/V_c	V_{exp}/V_c+V_f	V_{exp}/V_c	V_{exp}/V_c+V_f	V_{exp}/V_c
	kN		kN		kN		kN		kN									
GB580	13.1	-	29.3	-	27.5	-	15.9	-	23.9	2.16	-	0.97	-	1.03	-	1.79	-	1.19
GB590	13.7		30.8	-	28.9	-	17.1	-	26.7	1.83	-	0.81	-	0.87	-	1.47	-	0.94
GB58	12.7	-	28.1	-	26.3	-	16.4	-	24.7	2.94	-	1.33	-	1.42	-	2.28	-	1.51
GB58R	13.6	-	30.5	-	28.6	-	18.5	-	28.0	2.53	-	1.13	-	1.20	-	1.86	-	1.23
GB59R	13.7	-	30.8	-	28.9	-	18.8	-	28.4	2.21	-	0.98	-	1.05	-	1.61	-	1.06
GB62	14.0	10.9	31.7	11.0	29.7	2.8	19.6	8.8	26.9	-	1.93	-	1.13	-	1.48	-	1.70	-
GB63	13.9	11.8	31.3	11.9	27.1	3.1	19.3	9.5	26.5	-	2.11	-	1.25	-	1.79	-	1.88	-
GB54	17.6	-	35.2	-	34.0	-	21.6	-	30.7	1.78	-	0.89	-	0.92	-	1.45	-	1.02
GB55	17.6	-	35.2	-	34.0	-	18.0	-	27.1	2.69	-	1.34	-	1.39	-	2.63	-	1.74
GB64	19.9	15.3	41.0	15.5	39.4	4.0	22.5	11.6	34.0	-	1.75	-	1.09	-	1.42	-	1.81	-
GB65	19.9	16.9	41.0	17.1	37.6	4.4	22.5	12.7	34.0	-	1.72	-	1.09	-	1.51	-	1.80	-
GB56	24.6	-	47.2	-	43.6	-	29.4	-	41.7	1.78	-	0.93	-	1.01	-	1.50	-	1.05
GB57	24.4	-	46.6	-	43.1	-	26.0	-	38.2	2.05	-	1.07	-	1.16	-	1.92	-	1.31
GB60	24.7	17.5	47.3	17.8	42.3	4.6	24.6	12.4	37.2	-	1.83	-	1.19	-	1.65	-	2.08	-
GB61	24.7	16.9	47.3	17.1	40.5	4.4	24.6	11.9	37.2	-	2.06	-	1.33	-	1.90	-	2.33	-
Average										**2.22**	**1.90**	**1.05**	**1.18**	**1.12**	**1.63**	**1.83**	**1.93**	**1.23**
St Dev										**0.40**	**0.15**	**0.18**	**0.09**	**0.18**	**0.17**	**0.38**	**0.21**	**0.24**
COV										**0.18**	**0.08**	**0.17**	**0.07**	**0.16**	**0.11**	**0.21**	**0.11**	**0.20**

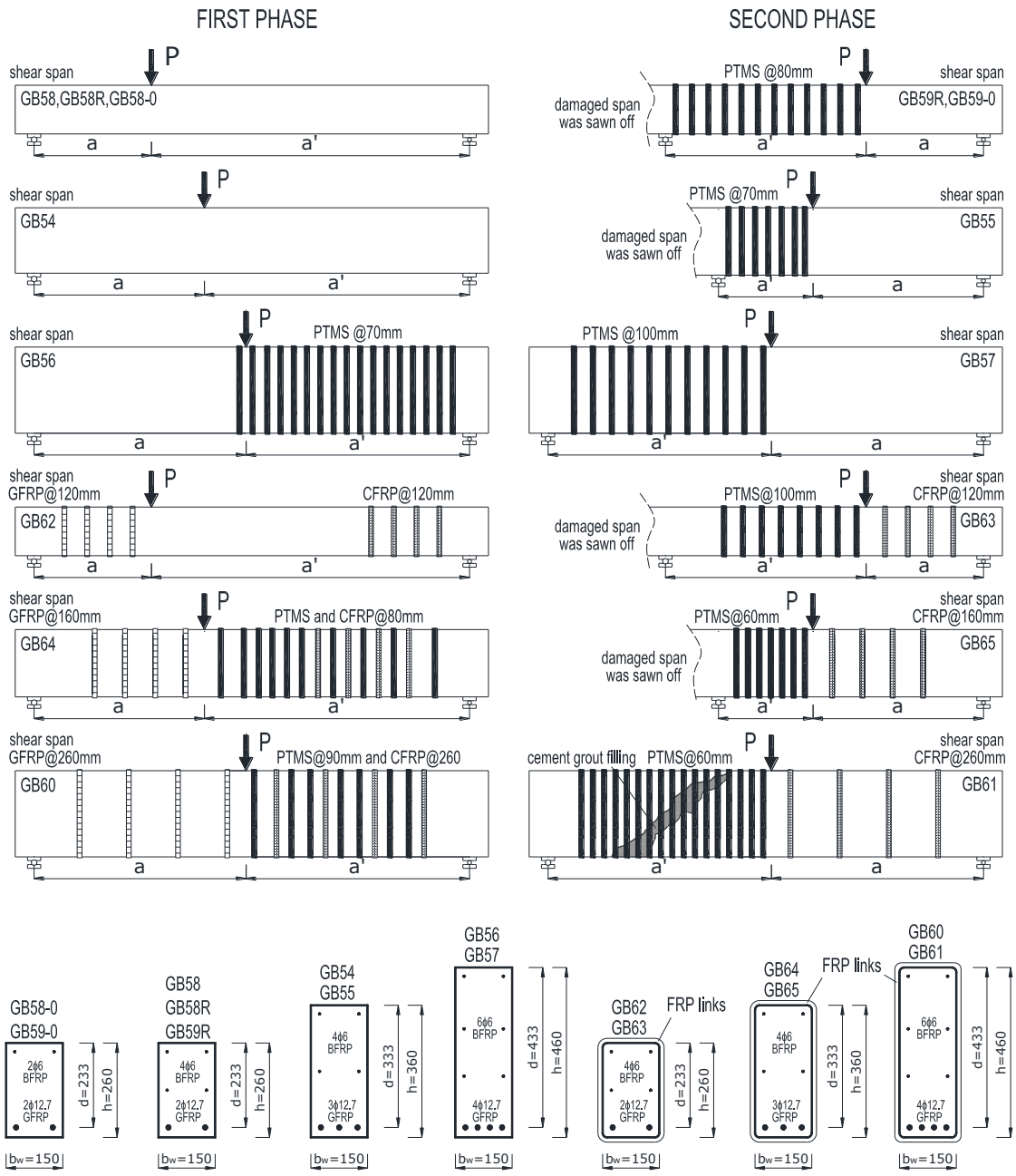
FIRST PHASE
SECOND PHASE
shear span
GB58,GB58R,GB58-0
damaged span was sawn off
PTMS @80mm
GB59R,GB59-0
GB54
PTMS @70mm
GB55
GB56
GB57
PTMS @100mm
GFRP@120mm
CFRP@120mm
GB62
GB63
GFRP@160mm
CFRP@160mm
PTMS and CFRP@80mm
PTMS@60mm
GB64
GB65
GFRP@260mm
CFRP@260mm
PTMS@90mm and CFRP@260
cement grout filling
GB60
GB61
GB58-0
GB59-0
GB58
GB58R
GB59R
GB54
GB55
GB56
GB57
GB62
GB63
FRP links
GB64
GB65
GB60
GB61
2φ6 BFRP
2φ12.7 GFRP
4φ6 BFRP
3φ12.7 GFRP
6φ6 BFRP
4φ12.7 GFRP
d=233
h=260
d=333
h=360
d=433
h=460
bw=150

Fig. 1

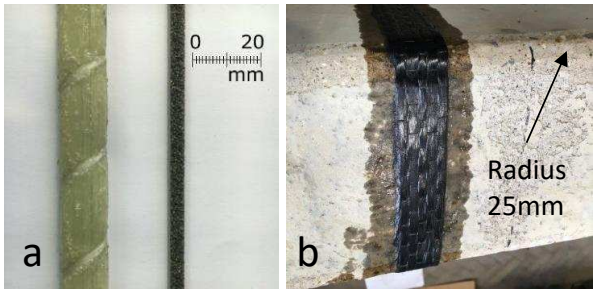
0 20
mm
a
b
Radius
25mm

Fig. 2

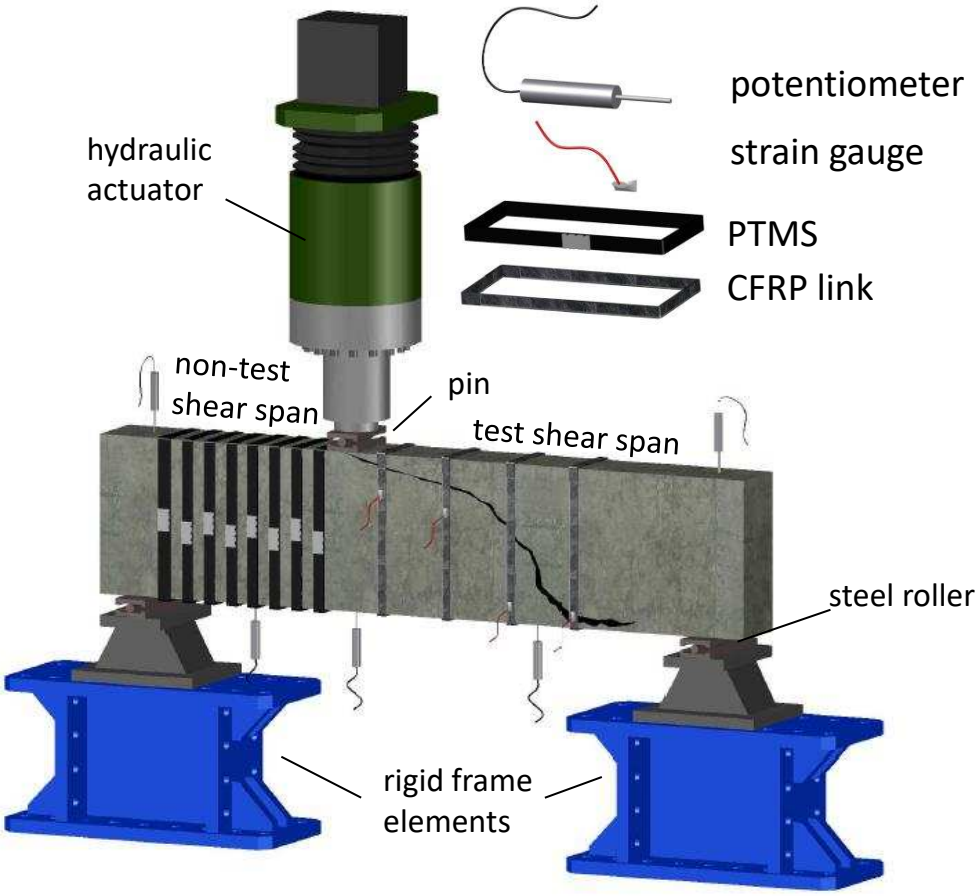
potentiometer
strain gauge
hydraulic
actuator
PTMS
CFRP link
non-test
shear span
pin
test shear span
steel roller
rigid frame
elements

Fig. 3a

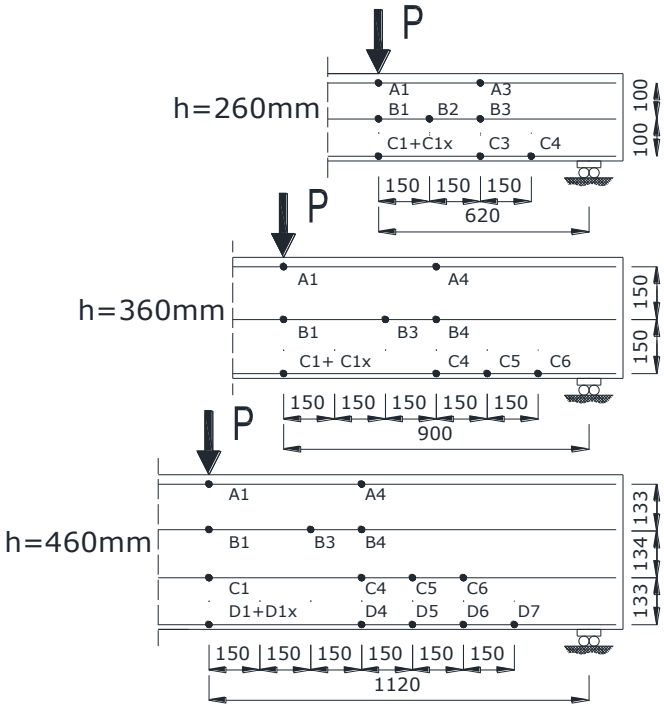
P
h=260mm
A1
A3
B1
B2
B3
C1+C1x
C3
C4
100
100
150 150 150
620
P
h=360mm
A1
A4
B1
B3
B4
C1+ C1x
C4
C5
C6
150
150
150 150 150 150 150
900
P
h=460mm
A1
A4
B1
B3
B4
C1
C4
C5
C6
D1+D1x
D4
D5
D6
D7
133
134
133
150 150 150 150 150 150
1120

Fig. 3b

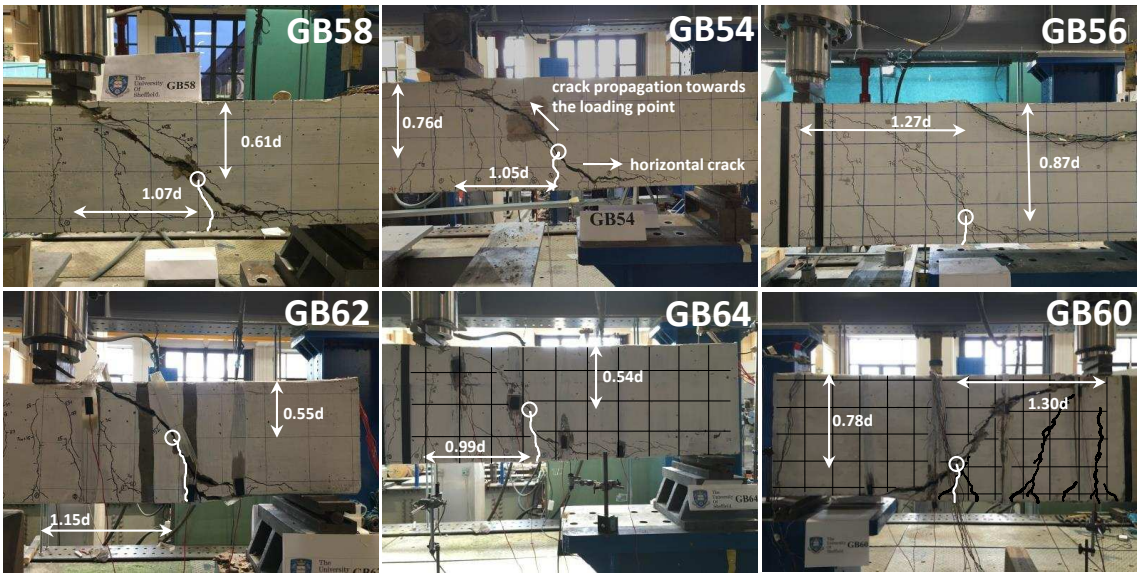
GB58
0.61d
1.07d
GB54
crack propagation towards the loading point
0.76d
1.05d
horizontal crack
GB54
GB56
1.27d
0.87d
GB62
0.55d
1.15d
GB64
0.54d
0.99d
GB60
0.78d
1.30d

Fig. 4

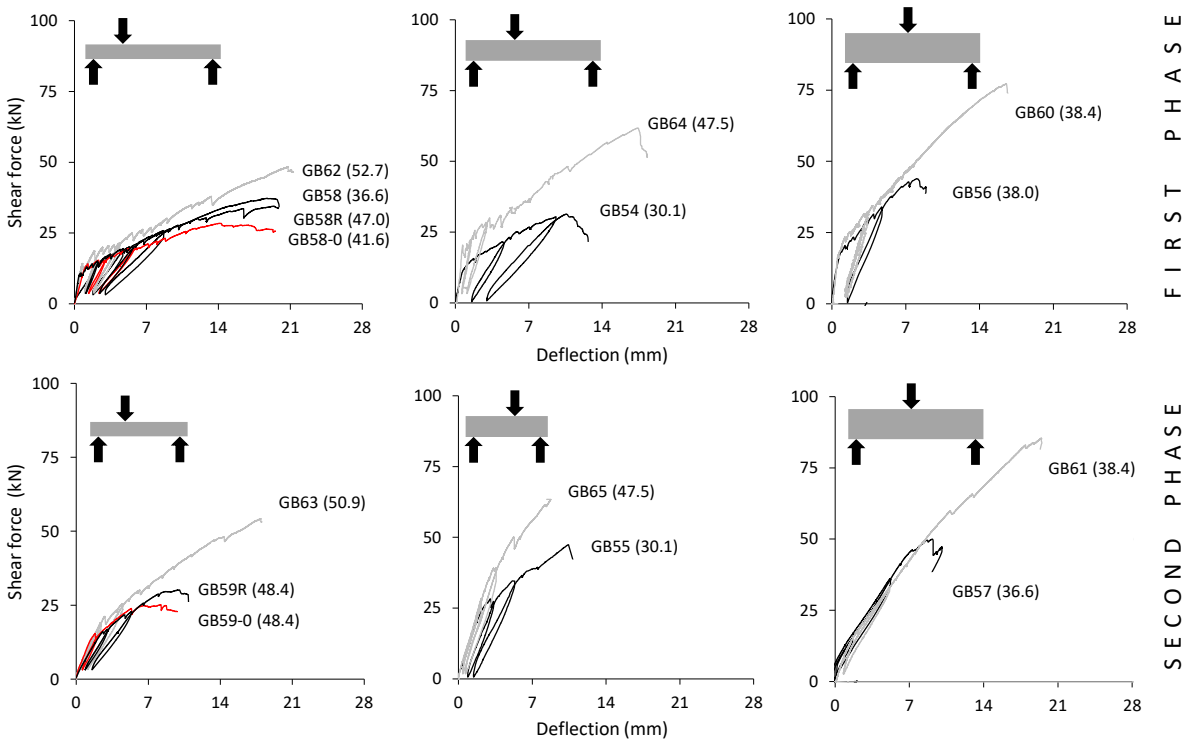
Shear force (kN)
Deflection (mm)
GB62 (52.7)
GB58 (36.6)
GB58R (47.0)
GB58-0 (41.6)
GB64 (47.5)
GB54 (30.1)
GB60 (38.4)
GB56 (38.0)
GB63 (50.9)
GB59R (48.4)
GB59-0 (48.4)
GB65 (47.5)
GB55 (30.1)
GB61 (38.4)
GB57 (36.6)
FIRST PHASE
SECOND PHASE

Fig. 5

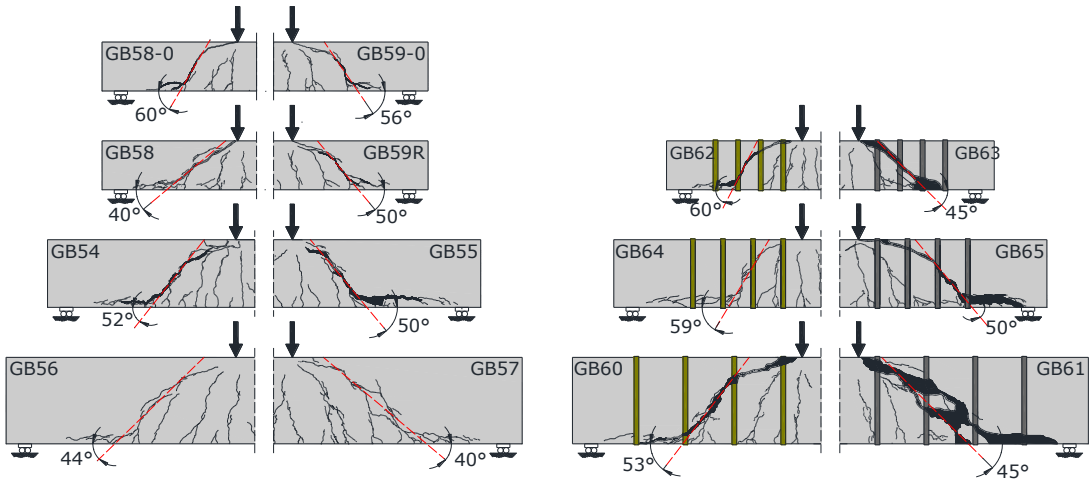
GB58-0
GB59-0
60°
56°
GB58
GB59R
40°
50°
GB54
GB55
52°
50°
GB56
GB57
44°
40°
GB62
GB63
60°
45°
GB64
GB65
59°
50°
GB60
GB61
53°
45°
a
b

Fig. 6

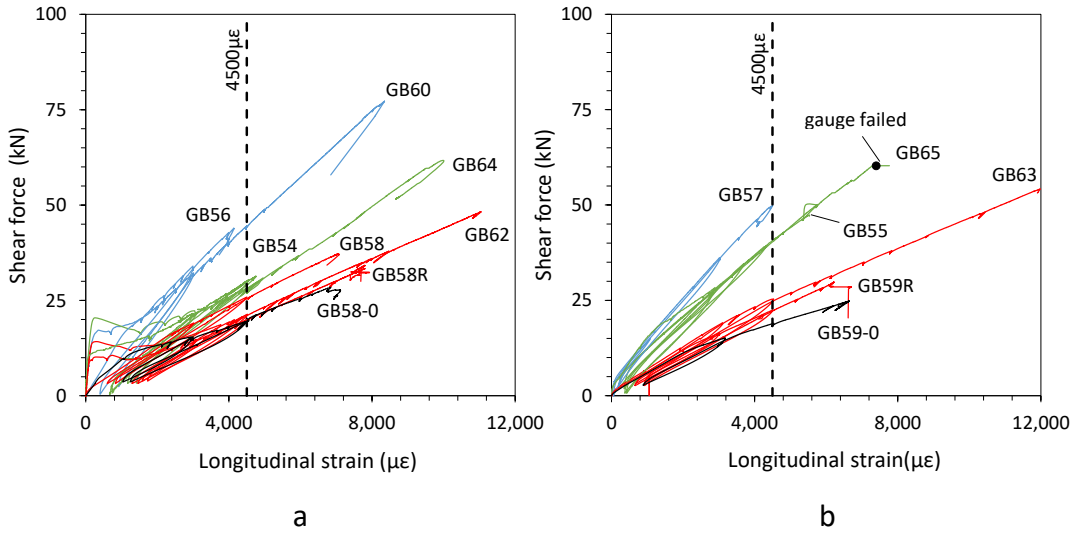
Shear force (kN)
Longitudinal strain (με)
4500με
GB60
GB64
GB56
GB54
GB58
GB62
GB58R
GB58-0
a
Shear force (kN)
Longitudinal strain(με)
4500με
gauge failed
GB65
GB63
GB57
GB55
GB59R
GB59-0
b

Fig. 7

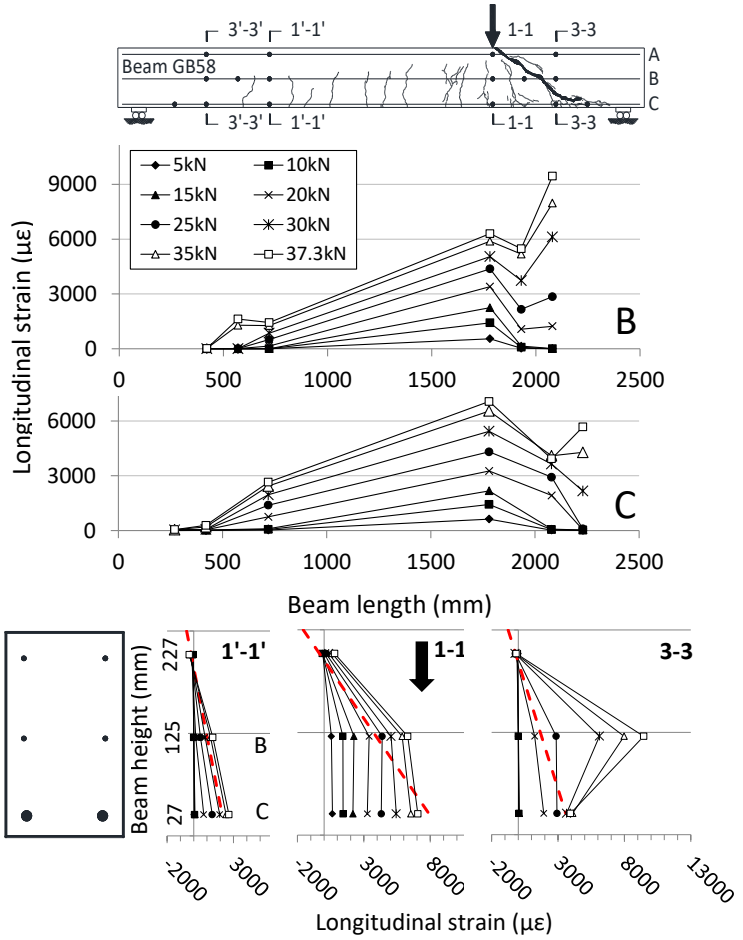
3'-3'
1'-1'
1-1
3-3
Beam GB58
A
B
C
5kN
10kN
15kN
20kN
25kN
30kN
35kN
37.3kN
Longitudinal strain (με)
Beam length (mm)
Beam height (mm)
1'-1'
1-1
3-3
227
125
27
Longitudinal strain (με)

Fig. 8

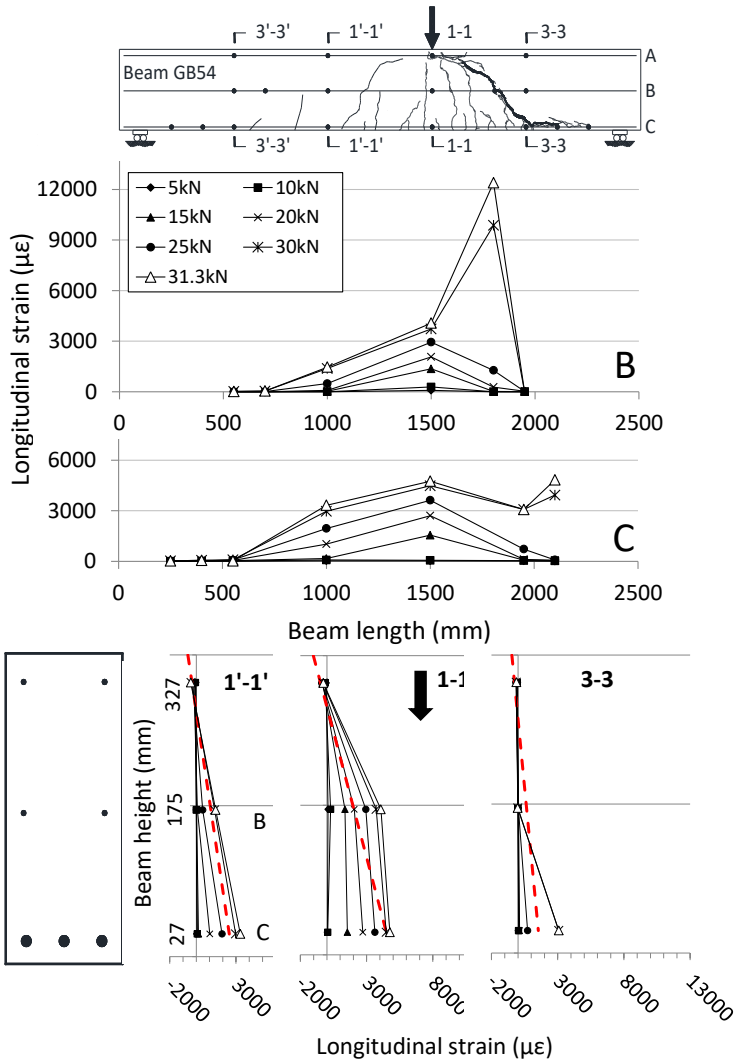
3'-3'
1'-1'
1-1
3-3
Beam GB54
A
B
C
5kN
10kN
15kN
20kN
25kN
30kN
31.3kN
Longitudinal strain (με)
Beam length (mm)
B
C
1'-1'
1-1
3-3
Beam height (mm)
327
175
27
Longitudinal strain (με)

Fig. 9

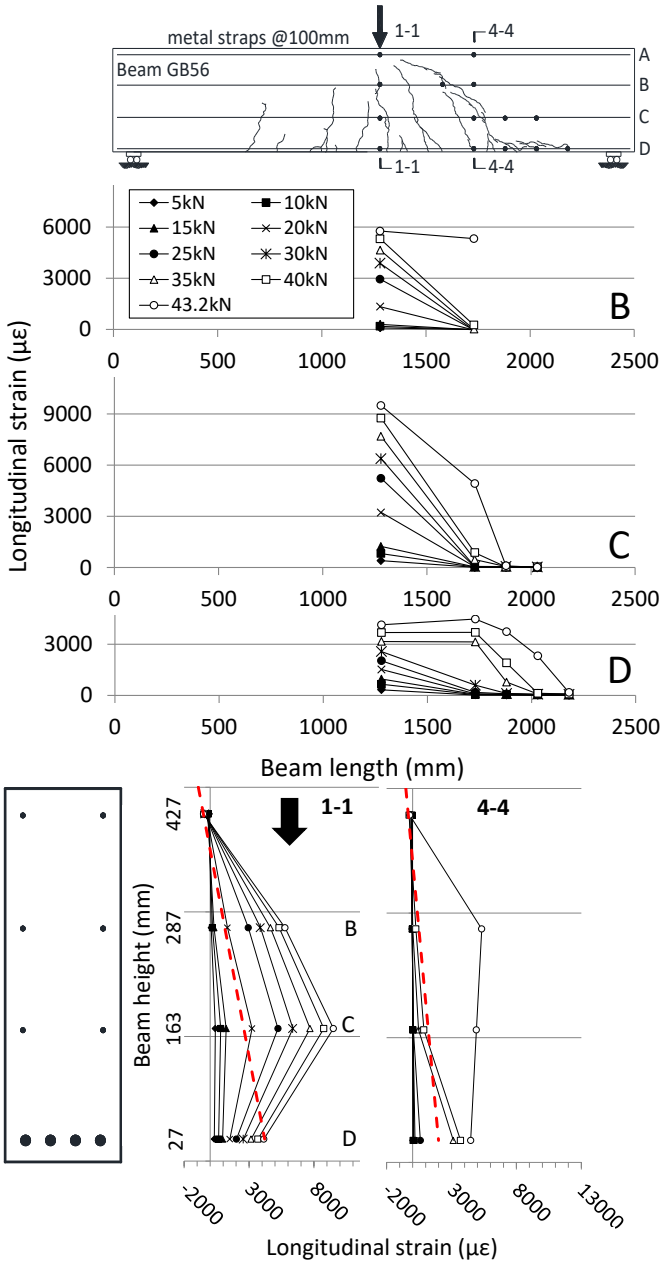
metal straps @100mm
1-1
4-4
Beam GB56
A
B
C
D
5kN
10kN
15kN
20kN
25kN
30kN
35kN
40kN
43.2kN
Longitudinal strain (με)
Beam length (mm)
Beam height (mm)
427
287
163
27
-2000
3000
8000
13000

Fig. 10

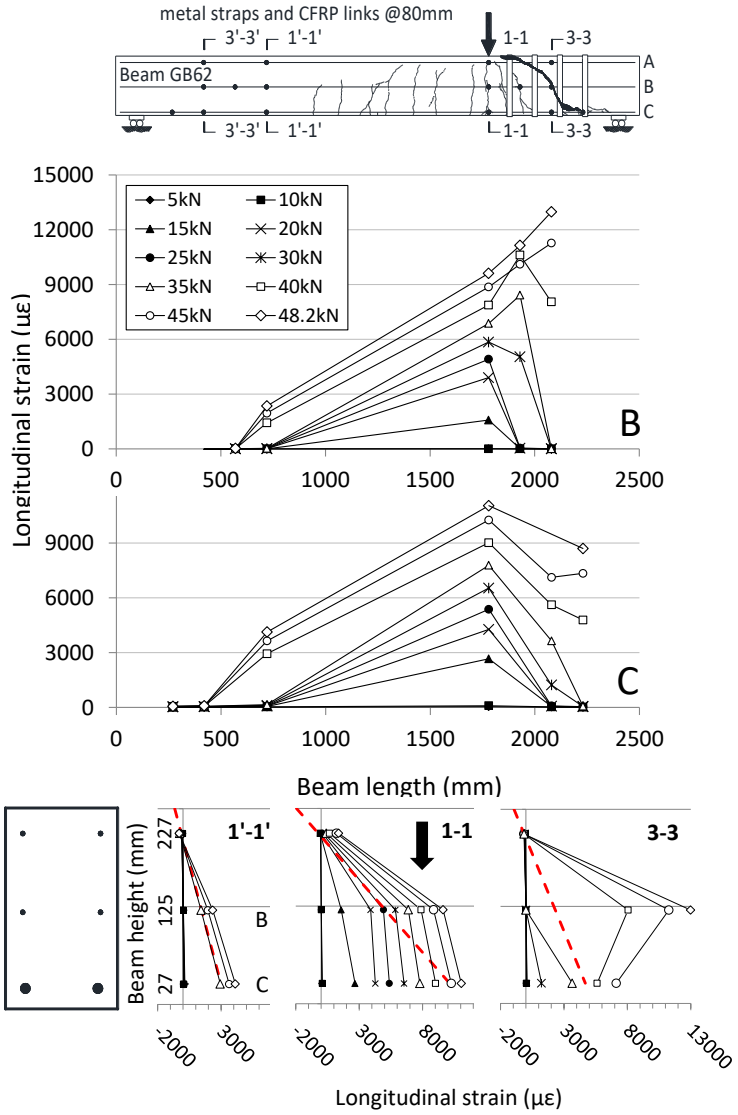
metal straps and CFRP links @80mm
3'-3'
1'-1'
1-1
3-3
Beam GB62
A
B
C
5kN
10kN
15kN
20kN
25kN
30kN
35kN
40kN
45kN
48.2kN
Longitudinal strain (με)
B
C
Beam length (mm)
Beam height (mm)
227
125
27
1'-1'
1-1
3-3
-2000
3000
8000
13000
Longitudinal strain (με)

Fig. 11

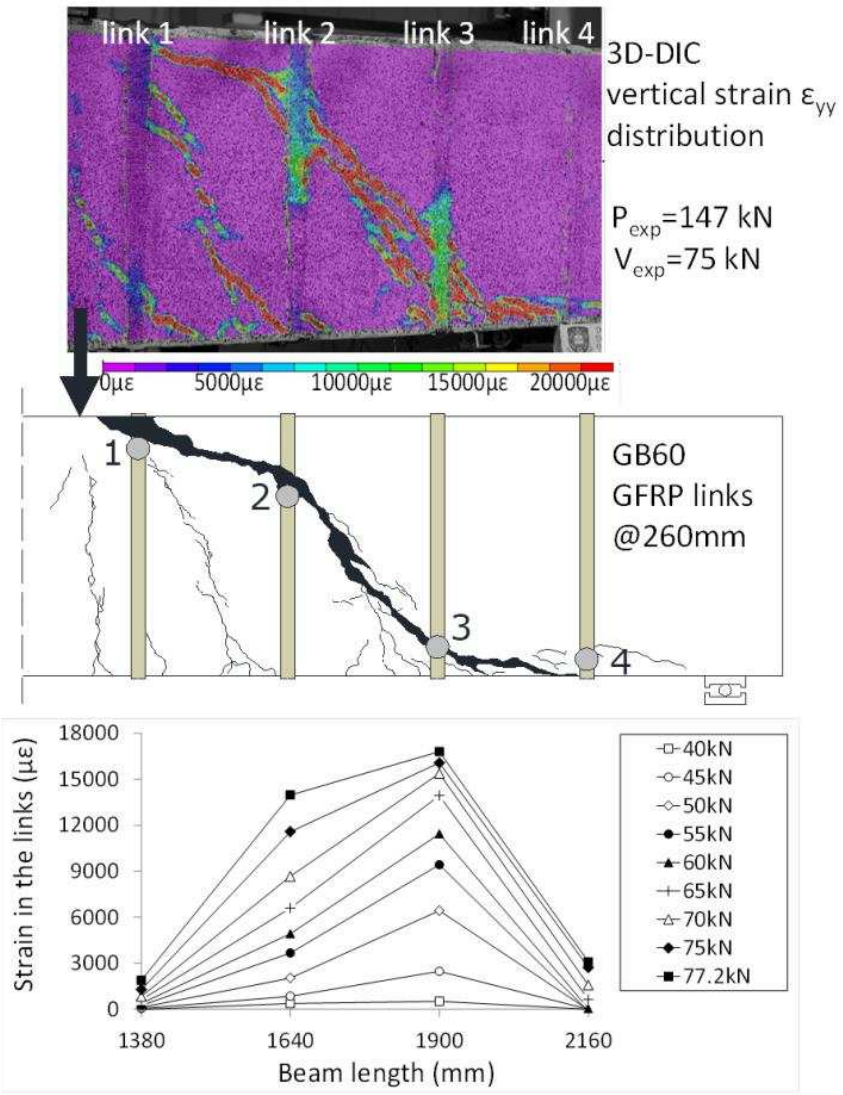
link 1
link 2
link 3
link 4
3D-DIC
vertical strain ε_{yy}
distribution
P_{exp}=147 kN
V_{exp}=75 kN
0με
5000με
10000με
15000με
20000με
1
2
3
4
GB60
GFRP links
@260mm
Strain in the links (με)
18000
15000
12000
9000
6000
3000
0
1380
1640
1900
2160
Beam length (mm)
40kN
45kN
50kN
55kN
60kN
65kN
70kN
75kN
77.2kN

Fig. 12

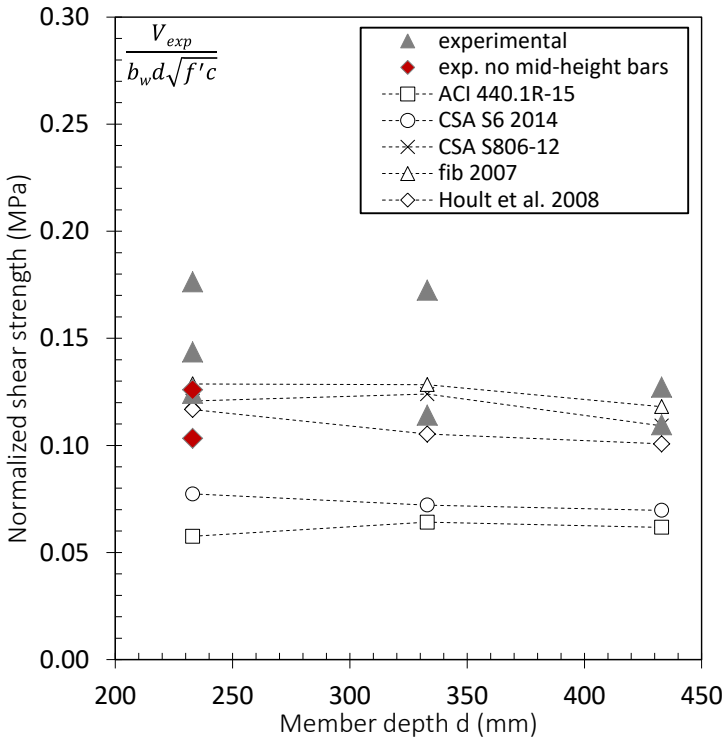

Fig. 13a

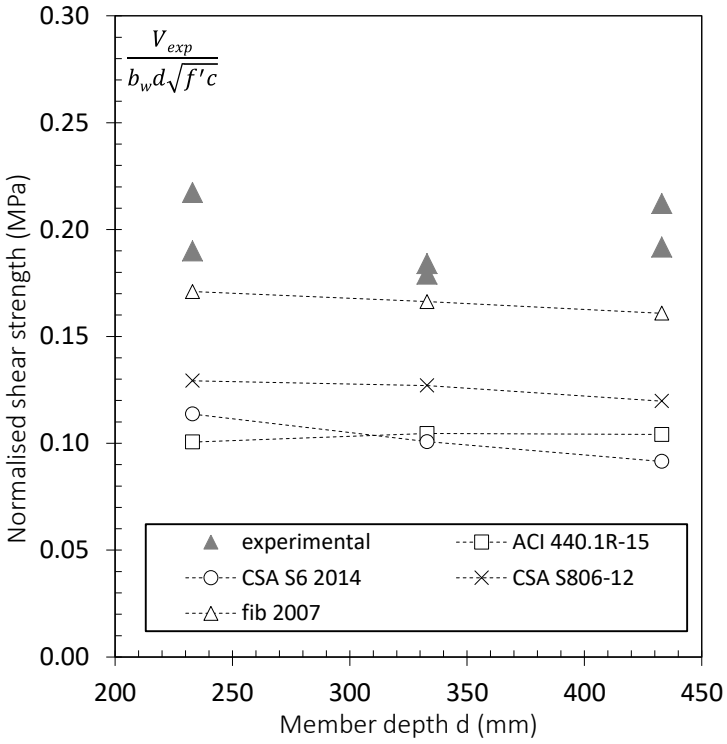

Fig. 13b